Assessment of ocular beta radiation dose distribution due to ^{106}Ru/^{106}Rh brachytherapy applicators using MCNPX Monte Carlo code

Nilséia Aparecida Barbosa[1], Luiz Antonio Ribeiro da Rosa[2], Artur Ferreira de Menezes[1], Juraci Passos Reis Júnior[1], Alessandro Facure[2, 3], Delson Braz[1]

[1]*Department of Nuclear Engineering, Universidade Federal do Rio de Janeiro, COPPE/UFRJ, Brazil.*
[2]*Division of Medical Physics, Instituto de Radioproteção e Dosimetria, Brazil.*
[3]*Coordination of Radioactive Facilities, Comissão Nacional de Energia Nuclear, Brazil.*

Original Article

Abstract

Purpose: Melanoma at the choroid region is the most common primary cancer that affects the eye in adult patients. Concave ophthalmic applicators with ^{106}Ru/^{106}Rh beta sources are the more used for treatment of these eye lesions, mainly lesions with small and medium dimensions. The available treatment planning system for ^{106}Ru applicators is based on dose distributions on a homogeneous water sphere eye model, resulting in a lack of data in the literature of dose distributions in the eye radiosensitive structures, information that may be crucial to improve the treatment planning process, aiming the maintenance of visual acuity. **Methods**: The Monte Carlo code MCNPX was used to calculate the dose distribution in a complete mathematical model of the human eye containing a choroid melanoma; considering the eye actual dimensions and its various component structures, due to an ophthalmic brachytherapy treatment, using ^{106}Ru/^{106}Rh beta-ray sources. Two possibilities were analyzed; a simple water eye and a heterogeneous eye considering all its structures. Two concave applicators, CCA and CCB manufactured by BEBIG and a complete mathematical model of the human eye were modeled using the MCNPX code. **Results and Conclusion:** For both eye models, namely water model and heterogeneous model, mean dose values simulated for the same eye regions are, in general, very similar, excepting for regions very distant from the applicator, where mean dose values are very low, uncertainties are higher and relative differences may reach 20.4%. For the tumor base and the eye structures closest to the applicator, such as sclera, choroid and retina, the maximum difference observed was 4%, presenting the heterogeneous model higher mean dose values. For the other eye regions, the higher doses were obtained when the homogeneous water eye model is taken into consideration. Mean dose distributions determined for the homogeneous water eye model are similar to those obtained for the heterogeneous eye model, indicating that the homogeneous water eye model is a reasonable one. The determined isodose curves give a good visualization of dose distributions inside the eye structures, pointing out their most exposed volume.

Keywords: Eye Brachytherapy; Monte Carlo; Dose Distribution; Ruthenium-106

Introduction

Beta radiation is the name given to energetic electrons emitted by the nucleus of unstable isotopes. Because of its physical characteristics, such as short range, resulting in large dose fall-off with distance and lower doses to the neighboring healthy tissues; beta radiation is largely used in brachytherapy applications as radiation sources for treatment of small lesions of the eye.[1]

^{90}Sr/^{90}Y and ^{106}Ru/^{106}Rh are the more used beta sources for the treatment of superficial tumors. Only ^{106}Ru/^{106}Rh applicators remain commercially available. They are used as concave applicators. The efficacy of such treatments, side effects and visual acuity long-term results are available in the literature.[1,2,3,4,5,7,8,9,10,11] Studies about conservation of eyesight after ^{106}Ru brachytherapy of choroidal melanoma show that

70% of patients with a tumor thickness not exceeding 3.0 mm had visual acuity of 20/40 or better in 5 years.[8]

Melanoma at the uvea region is the most common primary cancer that affects the eye in adult patients and its annual incidence is, approximately, six cases per one million people.[11] The use of enucleation decreased substantially during the last decades by the emergence of more conservative options, including brachytherapy with applicators, radiation treatment with charged particles, transpupillary thermotherapy, stereotactic radiosurgery and local resection.[12,13] Moore [14] was the first that used radon seed brachytherapy to preserve the vision for a monocular patient with uveal melanoma. Lommatzsch [4] pioneered the use of β-particles from ^{106}Ru/^{106}Rh and found that, as expected, "the severity and extension of post-radiation retinopathy is less than after ^{60}Co".

The usually recommended prescribed radiation dose to uveal melanoma control is between 80 to 100 Gy, specified at the tumor apex, depending on its size and location. The treatment period varies from two to fourteen days, depending on the source`s activity.[2,8,10] The choice of both the applicator model and the most adequate radionuclide for each treatment depends on a diversity of factors, including the proximity to optic nerve and fovea (center of macula), tumor shape, patient age during treatment and, mainly, height of the tumor apex.[8,9,10] Thus, the treatment plan, applicator model and radionuclide choice must optimize the dose distribution to minimize the treatment morbidity.[15]

According to the ICRU 72 and Collaborative Ocular Melanoma Study [1,16,17], the tumor thickness is defined as being the distance from the inner surface of the sclera to the apex of the tumor, the sclera is assumed to be 1mm thick. Tumors are classified as small if they are <3 mm in thickness and <10 mm in diameter; as medium-sized if they are 3- 5 mm in thickness and 10-15 mm in diameter and as large, if its dimensions are >5 mm in thickness and >15 mm in diameter. Large sizes tumors are usually treated by ophthalmic applicators emitting gamma-rays (either ^{103}Pd or ^{125}I).[18,19,20] For average and small sizes tumors, beta-ray applicators (^{106}Ru or ^{90}Sr) are preferred.[2,9,21]

The available treatment planning system for ^{106}Ru applicators is based on simplified physical models of radiation transport and on a very rough approximation of the anatomy of the eye, which is assumed to be a homogeneous water sphere.[22] The Monte Carlo method has been used widely in dosimetric research of the human eye with different radioisotopes (ophthalmic applicators), beta and gamma emitters.[23,24,25,26,27,28,29] This method is generally accepted as the most accurate approach for simulation of absorbed dose distributions, mainly in the presence of small radiation fields, like the ones used for eye irradiation.[29] However, the determination of dose distribution produced by ^{106}Ru beta applicators in eye is still a challenge and needs further improvements. Despite the existence of many publications, all of them are based on the same simplified homogeneous geometry of the eye described above. However, the human eye has different regions and materials and some of them with high radiation sensitivity, such as the lens and macula.[25] Thus, a complete eye model considering all present regions and their elemental compositions are required in order to carry out a more accurate dosimetric study.

Quantify the absorbed radiation dose accurately due to beta-rays near the surface of the ophthalmic applicators is not an easy task. In fact, it is significantly more complex when different regions and materials that compose the human eye are considered.

This paper proposes to calculate the dose distribution in a complete mathematical model of the human eye, using geometrical volumes, containing a choroid melanoma, considering the eye actual dimensions and its various component structures such as sclera, choroid, retina, vitreous humor, cornea, anterior chamber, lens, optic nerve, optic disc, macula, fovea and foveola. In order to simulate a real adult human eye, the elemental compositions and densities of the different parts of the eye as well as the tumor region located in choroid (choroidal melanoma) were considered.[1] The radioactive element considered for simulation was a ^{106}Ru/^{106}Rh beta emitter brachytherapy source, which is used as applicators.

Methods and Materials

Radionuclide ^{106}Ru/^{106}Rh

The ^{106}Ru is a β$^-$ emitter with maximum energy of E = 39.4 keV, with a half-life of $T_{1/2}$ = 368.2 d. It decays to ^{106}Rh with $T_{1/2}$ = 29.80s, before decaying to ^{106}Pd (stable) with a maximum beta energy of 3.54 MeV.[1] The radiation relevant to radiotherapy is the beta radiation of the radionuclide ^{106}Rh. The gamma radiation contributes only negligibly, 1% to the total dose in the target volume and therefore does not need to be taken into account.[15] The ^{106}Rh beta spectrum used in the simulations was taken from ICRU Report 72.[1]

Monte Carlo code-MCNPX

The Monte Carlo method is based on probabilistic concepts resulting from the interactions of individual particles (electrons, in the present study) migrating within complex geometries and various kinds of materials.[30] The method is applied in order to simulate random and individual trajectories through the medium taking into account physical parameters such as density, chemical composition of the materials, particles that will be simulated, and characteristics of the source. Monte Carlo code MCNPX comprehends a wide range of atomic numbers and materials [30], such as e.g. Ag and

soft tissue, which were used to model the applicators and eye geometry studied in the present work.

All inputs were modeled using the Monte Carlo code (MCNPX) version 2.5.0.[30] The *F8 tally (MeV) was used to score the energy deposited in each structure of interest. The simulations were carried out considering the transport of electrons until the relative error converge to levels below 5% thus ensuring reliable results according to the limits of reliability presented in the guide interpretation relative error on MCNP.[31]

Geometric shape, dimensions and mathematical modeling of the ^{106}Ru/^{106}Rh applicators

The ^{106}Ru/^{106}Rh applicators simulated in this work are concave CCA and CCB types, produced by the BEBIG Eckert & Ziegler BEBIG GmbH.[15] These applicators models are the most commonly used for the treatment of uveal and choroidal melanomas of small and medium sizes.[1,27,29] Their geometric parameters and radiation activities are presented in **Table 1.**

The mathematical model of the applicators was defined as three concentric spherical shells of 24 mm internal diameter.

The pure silver inner spherical shell has a thickness of 0.1 mm (silver window), this window stop all the low-energy (E_{max} = 39 keV) beta particles from ^{106}Ru source. The next spherical shell presents a silver thickness of 0.2 mm with a 0.1 μm thickness layer of the radioisotope (^{106}Rh) electrolytically deposited on the concave surface. The outer spherical layer, the base of the applicator (silver support), has a thickness of 0.7 mm. These three spherical shells were cut by two cones with an aperture of α = arcsine (R/R_c), where R and R_c are the internal radius of the applicator and the curvature radius of the inner surface, respectively. The geometry of the applicator is presented in **Figure 1**. In this work, the source was assumed to have a uniform distribution of the radioactive material over its active area.

Dosimetric characteristics of ^{106}Ru/^{106}Rh eye applicators

According to the manufacturer manual, the radiation absorbed dose rate in water due to the ^{106}Ru/^{106}Rh applicators was measured with a plastic scintillation detector having high spatial resolution. Its calibration is based on the NIST (National Institute of Standards and Technology, USA) primary standard for radiation absorbed dose to water for beta radiation sources.[15]

TABLE 1: Geometric parameters and activities of the ^{106}Ru/^{106}Rh eye applicators[15]

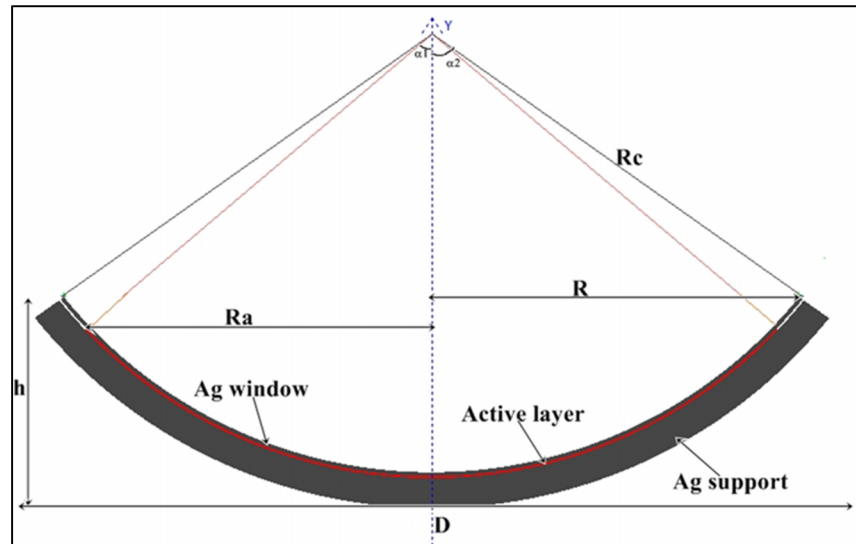| Type	Diameter (D) (mm)	Active Diameter (D_a) (mm)	Height (h) (mm)	Radius of curvature (R_c) (mm)	Nominal activity
CCA	15.3	13.0	3.3	12	10.0 MBq
CCB	20.2	17.8	5.4	12	19.0 MBq

FIG. 1: Mathematical model scheme of the ^{106}Ru/^{106}Rh applicators.

The expanded measured uncertainty of the dose values provided by the manufacturer is ±20% (95% confidence level).

The calibration data of the depth dose rate distribution (11 measurement points along the applicator symmetry axis,

from 0 to 10 mm) and the relative dose rate distribution at a 1 mm distance from the applicator surface (33 measurement points) are presented in the source calibration certificate. According to the source manufacturer data, these applicators were produced with a nominal reference dose rate of 80 mGy/min at a source-measurement point distance of 2 mm on the applicator symmetry axis. This value is equivalent to a surface dose rate of approximately 120 mGy/min. Applicators production-related deviations from nominal values ranging from -10% to +60% are possible.[15]

Aiming the validation of the Monte Carlo simulations carried out in the present work, percent depth dose curves (PDD), dose lateral profiles and isodoses curves in water were determined and compared to the results obtained using the data from the manufacturer manual and source certificate, as well as to the data presented by Hermida-López.[37]

In this study, aiming the calculation of radiation dose distributions in water, percent depth dose curves (PDD), dose lateral profiles and isodoses curves were determined. It was constructed a grid composed of 2.432 bins of $0.15 \times 0.15 \times 0.15$ mm³. The grid ranged from -13.30 to 13.30 mm in the lateral axis and from 1.85 to 13.05 mm in depth axis, sweeping, inclusively, the outer area of the applicator. This grid was placed on the depth axis of the applicator that was attached to a water sphere, representing the eyeball.

In order to calculate the relative dose distributions in depth and laterally, considering each applicator, eleven positions of dose evaluation were marked at the grid, in intervals of 1 mm along the axis of symmetry of the applicator, from the applicator's inner surface. The lateral dose distributions were determined for six depths, 1, 2, 3, 4, 6, and 8 mm, in lateral intervals of 1 mm. The relative doses have been normalized to 100% at a depth of 2 mm.

Eye anatomy and mathematical model of the eye and tumor

The adult human eye has, in average, 24.0 mm in diameter.[1,20,35] The outer coat consists of the opaque *sclera*, with a thickness of 0.3 - 1.0 mm and a diameter of 24.0 mm. The *uvea* (middle coat) is formed by the choroid (thickness of 0.1- 0.3 mm), the *ciliary body* (mid-zonal portion, thickness of 2.0 mm) and the *iris* (anterior portion, thickness of 0.5- 3.0 mm), which represents the origin of different types of uveal melanoma.

The inner coat consists of the *retina*, including the retinal pigment epithelium (thickness 0.1 mm). The *vitreous humor*, filling the inner part of the globe, does not contain any vital cells. It is composed of 99% of water. The *optic nerve* enters the globe at the optic disc (papilla of the optic nerve). The *macula* (4.0 mm diameter) represents anatomically the cen-

tral portion of the retina with the highest concentration of visual cells and is therefore the most important structure for the visual acuity. The *lens*, which have a density of 1.07 g/cm³, separate the vitreous from the anterior chamber filled with aqueous humor.[1] **Figure 2** shows the anatomy of the eye.
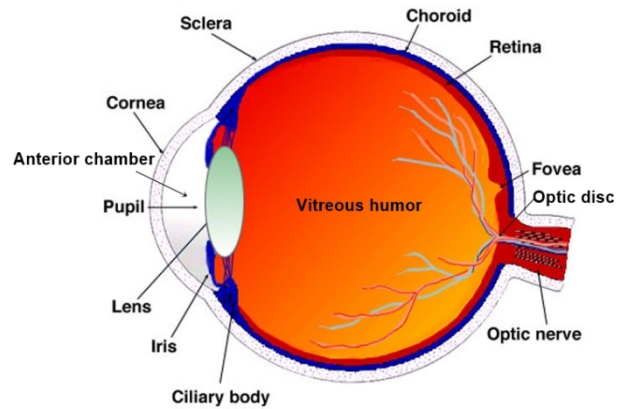

FIG. 2: The human eye diagram (COMS).

In the eye mathematical model considered, using as reference the dimensions of the eye model presented in AAPM and ABS Task Group 129 Report [20], the eye globe has been defined as four concentric spherical shells centered at the origin of the coordinates system (**Figure 3**). This anatomy is composed of three layers including the eye body, namely the *sclera* (outer) with diameter of 24.0 mm and thickness of 1.0 mm, *choroid* (middle) with diameter of 23.0 mm and thickness of 0.3 mm, *retina* (inner) with 22.0 mm diameter and thickness of 0.1 mm. The *vitreous humor* is the spherical region limited by the inner surface of the retina.

The tumor region has been defined as an ellipsoid, cut by the spherical surface of choroid, forming a semi-ellipsoid, dome-shaped, situated inside the eye. The tumor spreads in the interior of the retina and vitreous humor, with a thickness of 4.0 mm and a basal diameter of 13.0 mm (**Figure 3**).

The *cornea* was modeled as an elliptical shell limited by two concentric ellipses, situated at the outer surface of the choroid with a thickness of 0.5 mm. The *optic nerve* and its wall are represented, by a cylinder and a cylindrical shell, respectively, concentrically localized. Both extend from the outer sclera surface, rotated by 20° in relation to the coordinate system (**Figure 3**).

The *lens* was represented as an ellipsoid having its center localized 8.0 mm from the coordinate system center. The anterior chamber is the geometric region between the surface that defines the cornea inner wall and the outer surface of the vitreous humor (**Figure 3**).

The *macula* is a disk-like structure with 4.0 mm in diameter situated within the retina. The *fovea* is a depression in the center of the macula, having a structure disk-like of 1.5 mm in diameter. In its center there is a depression of about 0.35 mm in diameter, designated by *foveola*. The *optic disc* (papilla) is the part of the optic nerve that protrudes into the back of the eye; being a slightly oval structure with 1.8 mm in diameter, located in both the sclera and retina (**Figure 3**).

Materials, elemental composition and density of each eye component are shown in **Table 2**. For comparison, the eye regions were also simulated considering that they were composed only by water, with density of 1.0 g/cm³.

The *F8 tally of MCNPX provides the energy deposited in a cell, in MeV. In order to convert the results of the *F8 tally in mGy/min, that is, absorbed dose rate in tissue, the results from *F8 tally were divided by the mass (g) of each eye anatomical structure (cell), including the tumor, multiplied by the unit conversion factor (9.61×10^{-3} J.kg^{-1}.min^{-1}), considering 1 MBq as the source activity. For different activity values in MBq, the results should be multiplied by these values, equation (1).

$$\dot{D} = \frac{{}^{*}F8}{M}A \qquad (1),$$

Where $\dot{D}$ is the dose rate in mGy/min, *F8 is a MCNPX tally command that provides the deposited energy in MeV, A is the source activity in Bq and M is the mass in g.

All inputs were simulated for a total of 2×10^{8} electron histories, resulting in statistical uncertainties generated by *F8 tally lower than 1%.

TABLE 2: Density and elemental composition of each eye region.[35,36]

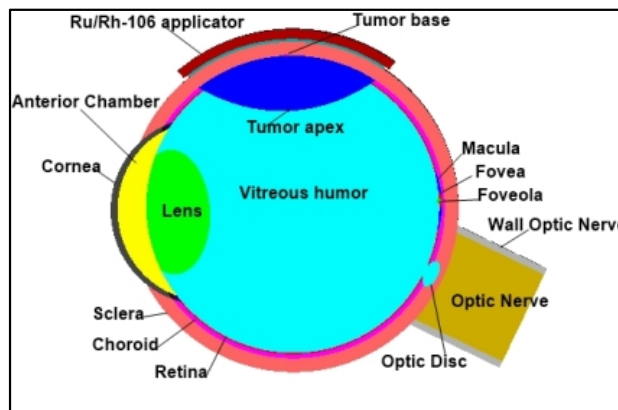| Sclera, choroid, Retina, Cornea, Optic nerve and Wall, Macula, Optic disc, Fovea, Foveola and Tumor. Soft tissue: (1.04 g/cm³)	Percent by weight	Lens (1.07 g/cm³)	Percent by weight	Vitreous body and anterior chamber Water:(1g/cm³)	Percent by weight
H	10.454	H	9.6	H	0.112
C	22.663	C	19.5	O	0.888
N	2.490	N	5.7	-	-
O	63.525	O	64.6	-	-
Na	0.112	Na	0.1	-	-
Mg	0.013	P	0.1	-	-
Si	0.030	S	0.3	-	-
P	0.134	Cl	0.1	-	-
S	0.204	-	-	-	-
Cl	0.133	-	-	-	-
K	0.208	-	-	-	-
Ca	0.024	-	-	-	-
Fe	0.005	-	-	-	-
Zn	0.003	-	-	-	-
Rb	0.001	-	-	-	-
Zr	0.001	-	-	-	-

FIG. 3: Coronal view of the simulated eye and tumor, 2D.

Results

Relative Depth Dose and Lateral Dose Distributions Using MCNPX

Relative depth dose and lateral dose profiles were tallied along the symmetry axes of the applicators, extending from the inner concave surface into the water sphere. The **Figures 4, 5 and 6** show the relative depth dose and lateral profile dose distributions along distances perpendicular to the symmetry axis at different depths, simulated with MCNPX *F8 tally, for both CCA and CCB applicators compared with experimental data provided by the manufacturer, BEBIG, and with the MC-PENELOPE calculations carried out by Hermida-López [37], whose results were well discussed and compared with those of other authors.[32,33,34]
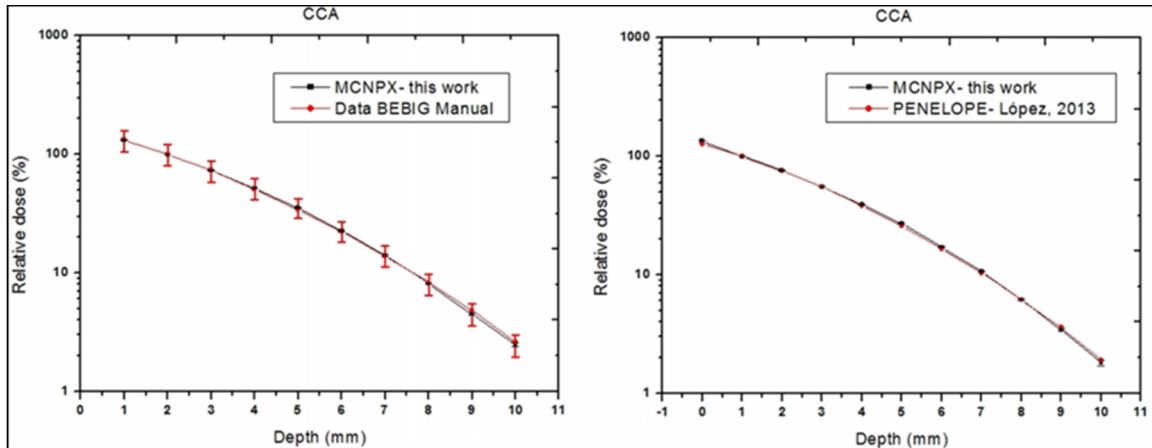

FIG. 4: Central axis depth dose curves for CCA applicator: Comparison between BEBIG GmbH manufacturer manual data and MCNPX (present work) results (left Figure). Comparison between PENELOPE/Hermida-López [37] simulations and MCNPX (present work) results (right Figure). The relative doses have been normalized to 100% at a depth of 2 mm (left figure) and 100% at a depth of 1 mm at the central axis (right Figure).

FIG. 5: Central axis depth dose curves for CCB applicator: Comparison between BEBIG GmbH manufacturer certificate data and MCNPX (present work) results (left Figure). Comparison between PENELOPE/Hermida-López [37] simulations and MCNPX (present work) results (right Figure). The relative doses have been normalized to 100% at a depth of 2 mm (left Figure) and 100% at a depth of 1 mm at the central axis (right Figure).
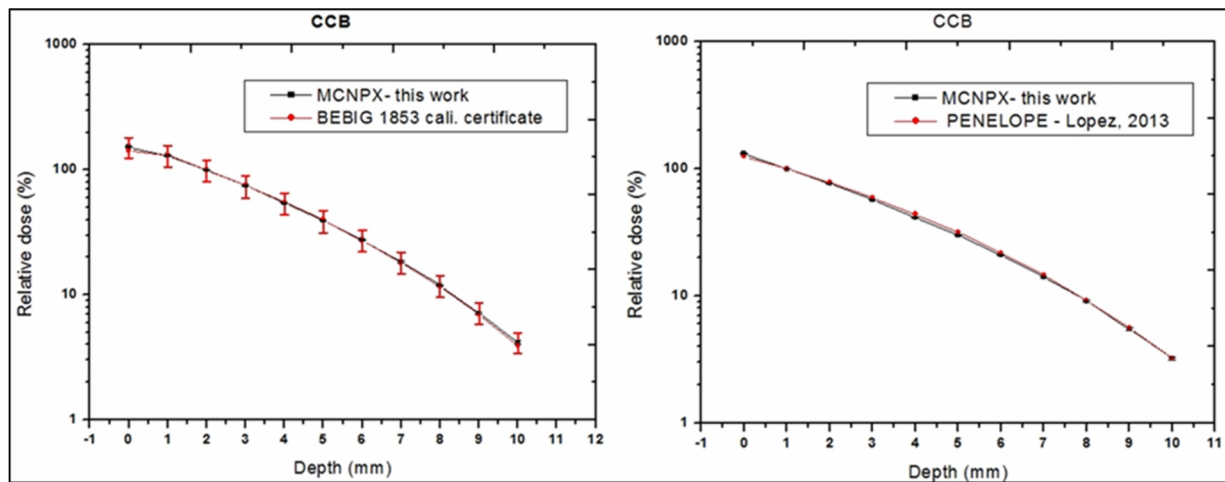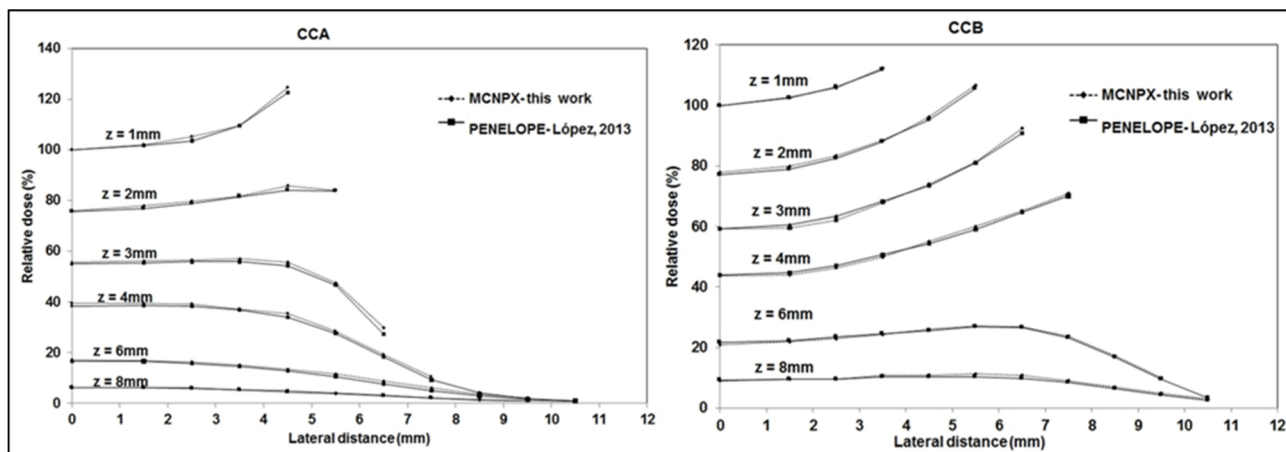

FIG. 6: Lateral dose distributions calculated using MCNPX at 1, 2, 3, 4, 6, and 8 mm depths for CCA (left figure) and CCB (right figure) applicators. The data are compared to PENELOPE/Hermida-López [37] results. The relative doses have been normalized to 100% at a depth of 1 mm at the central axis.

Figures 4 and 5 show a good agreement between the results obtained in this work and the data using the manufacturer-BEBIG certificate and manual[15] and simulated by Hermida-Lopéz [37] (within the statistical uncertainty, 20% for data obtained using the manufacturer manual and 1% for both Monte Carlo procedures, present work and obtained by Hermida-López)[37]. The largest differences were found at depths 4 e 5 mm. For example, for CCB applicator, at 4 mm depth, the relative dose obtained by Hermida-López is 44%, while, in the present work, the relative dose value found is 43%. For CCA applicator, at 5 mm depth, the relative dose calculated by Hermida-López is 25.8% and the value determined in this work is 26.8%. These results validate the MCNPX Monte Carlo Code used in the present work. However, comparing MCNPX results with manufacturer data, some larger discrepancies were found. For example, at the surface of CCB applicator, a difference of 6 % was determined and for CCA applicator, at depths 9 and 10 mm, a difference of 8% was found. One should have in mind that manufacturer data uncertainties are about 20 %, a value higher than those found to percent differences between manufacturer data and MCNPX results. Other authors had already found similar differences comparing Monte Carlo data and manufacturer data.[27,32,33]

Assuming the nominal activity values presented in **Table 1**, dose rates in the center of the surface of applicators CCA and CCB were, respectively, 96.4 and 129.1 mGy/mim. Using the calibration certificate of the CCB-1853 applicator, it was determined a dose rate of 128.3 mGy/min (dose rate corrected by source decay in 2013) in the center of the applicator surface, indicating a good agreement between Monte Carlo and certificate values. This comparison couldn´t be done for CCA applicator because its certificate wasn´t available.

Dose distribution in the eye

The MCNPX *F8 tally was used to quantify the energy deposition in the choroidal melanoma and all eye structures regions.

Table 3 shows the dose rates to the tumor apex and the tumor base, as well as the mean doses rate values in all structures at risk of the eye, such as sclera, choroid, retina, vitreous humor, optic nerve, optic nerve wall, cornea, anterior chamber, optic disc, lens, macula, fovea and foveola; calculated by simulating ophthalmic applicators of $^{106}Ru/^{106}Rh$, CCA and CCB models, attached to the human eye model considered in this work.

For comparison, were considered two eye models, namely one composed by real heterogeneities of the eye and another entirely composed of water.

Observing **Table 3**, considering the two types of applicators, it is possible to find that, for both eye models, namely water model and heterogeneity model, mean dose values calculated for the same structures are, in general, very similar, excepting for structures very distant from the applicator, where dose values are very low, uncertainties are higher and relative differences may reach 20.4 %. For the tumor base and the eye structures closest to the applicator such as sclera, choroid and retina, the most important structures for the treatment considered, the maximum difference observed was 4 %. For these structures, higher mean dose values are found when the heterogeneous model is considered. For the other eye structures, the higher mean doses are determined when the homogeneous water eye model is taken into consideration.

TABLE 3: Dose rate, $\dot{D}$(mGy/min), obtained by simulation with MCNPX, at the structural regions of the eye, considering a water eye model and an eye model with actual heterogeneities.

| Eye structures	Mass(g)	Plaque CCB Dose Rate [mGy/(min MBq)]			Plaque CCA Dose Rate [mGy/(min MBq)]		
		Heterogeneous eye model	Water eye model	Relative difference(%)	Heterogeneous eye model	Water eye model	Relative difference(%)
Tumor-apex	0.277	36.81	38.27	-3.4	22.80	23.98	-3.5
Tumor-base (inner sclera)		99.50	95.67	3.8	71.27	68.52	3.9
Lens	0.15	1.04	1.06	-1.9	0.160	0.165	-2.9
Anterior chamber	0.185	0.67	0.69	-3.0	0.083	0.087	-4.8
Cornea	0.177	0.35	0.36	-2.8	0.045	0.046	-2.2
Vitreos humor	4.53	6.26	6.40	-2.3	1.80	1.86	-3.3
Retina	0.149	7.55	7.43	1.6	1.33	1.31	1.5
Choroid	0.461	7.60	7.50	1.3	1.23	1.22	0.8
Sclera	1.730	18.72	18.32	2.1	7.28	7.12	2.2
Optic nerve (ON)	0.269	7.84E-03	7.81E-03	3.8	2.70E-03	2.69E-03	0.37
Optic nerve wall	0.086	9.30E-03	8.50E-03	8.6	2.74E-03	2.67E-03	2.6
Macula	1.76E-03	1.46E-02	1.56E-02	-6.7	1.58E-02	1.60E-02	-1.27
Optic disc	2.18E-03	1.20E-02	1.30E-02	-8.0	2.70E-03	2.80E-03	-3.70
Fovea	8.43E-04	3.82E-02	4.60E-02	-20.4	2.64E-03	3.16E-03	-19.7
Foveola	2.32E-05	4.09E-02	4.10E-02	-0.4	7.22E-02	7.30E-02	-1.1
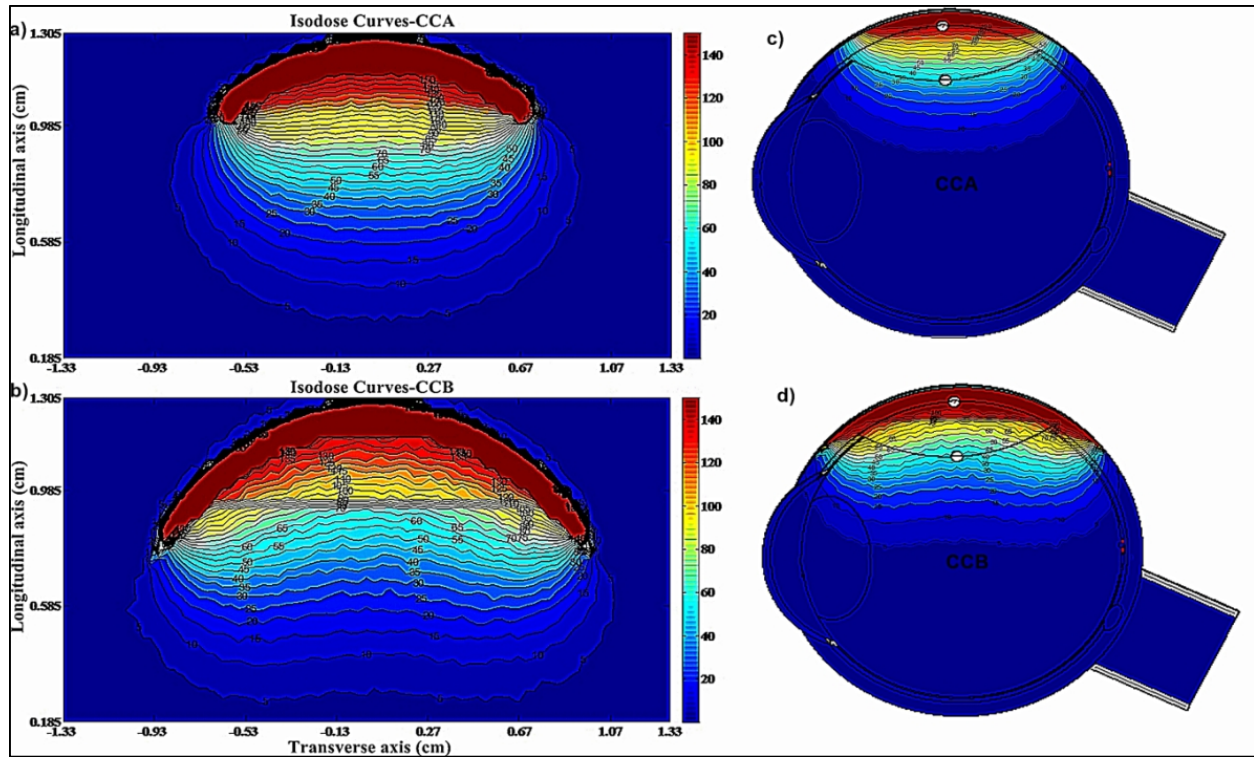
FIG. 7: Relative isodose distributions due to CCA and CCB applicators. The relative doses have been normalized to 100% at a depth of 2 mm. Figures (a) and (b) present the dose distributions in water, disregarding the eye presence. Figures (c) and (d) present dose distributions due to the same applicators inside the water eye model.

Considering that dose rate values provided by the applicators manufacturer calibration certificate present an uncertainty about 20 %, to consider the homogeneous water eye model for mean dose distribution simulation aiming treatment planning is reasonable.

The mean dose rate values presented in **Table 3** can give a rough idea about dose distribution in the eye, as whole, indicating the high dose gradient presented by ^{106}Ru/^{106}Rh beta source. However, in radiotherapy it is important to know the volumetric dose distribution for each important structure. For the applicator/eye geometry considered in the present work, dependent of the tumor position, one can find that mean dose values don´t describe properly the dose distribution in the sclera, choroid and retina. Considering **Figure 7**, which presents the isodoses distribution in the eye, it is possible to observe, for example, that higher dose values are concentrate at the upper part of the eye lens, being a mean dose value not representative of volumetric dose distribution inside the structure. The lower part of the structure practically is exposed to very low doses. In the cases of sclera, choroid and retina, the isodose curves give a good visualization of the parts of these structures more exposed to the radiation treatment. Naturally, the present discussion is valid for the special applicator position considered. For other tumor positions, consequently other applicator localization, new analysis are requested and different structures may receive higher doses. Obviously, sclera, choroid and retina will always be exposed to high doses.

Figures 7 (a) and **(b)** display the isodose distributions simulated for the CCB and CCA applicators in water, along applicator axis as a function of the transverse distance.

The isodose plots highlight the differences between the dose profiles produced by both applicators. The dose distribution for CCA applicator decreases uniformly along the applicator symmetry axis and a large lateral dose fall-off is observed, while the CCB applicator lateral dose distribution fall-off doesn't decrease so rapidly. This difference can be, mainly, due to the different extensions of the active regions in both applicators.

The goal of a radiation treatment is to minimize doses to healthy tissues with recommended maximum dose to the tumor. Therefore, the doses to the critical structures are crucial for the risk of side effects, especially for maintaining visual acuity. Uncertainty in the tumor location is another critical factor. The risk of local recurrence increases for tumors close to the optic disc or fovea/macula.[38] Considering the wealth of detail with which the eye model was constructed in this work, it is possible to estimate the dose for any of these structures, with the flexibility to vary the tumor dimensions and locations, applicator position and thus verify the doses in critical structures near the tumor.

Once dose rates fall-off rapidly in the more distant structures from the applicator, due to the limited range of the electrons in tissue, there is a limitation of tumors size that are able to be reasonably treated with such applicators; justifying the important therapeutic indication of the ^{106}Ru/^{106}Rh applicators for small and medium tumors.[3,5,7,8,9]

Discussion and Conclusions

The simulated results obtained with the use of MCNPX Monte Carlo code for mean doses rates distributions in a complete mathematical model of the human eye for two ^{106}Ru/Rh^{106} applicators, CCA and CCB, show that the correct choice of the applicator model, the knowledge of the thickness and tumor localization and the prescription dose are fundamental in order to provide an effective treatment.

Mean dose rate distributions were simulated in two eye models composed only by water and considering eye heterogeneities. For the tumor base and the eye structures closest to the applicator such as sclera, choroid and retina, the most important structures for the treatment considered, the maximum difference observed was 4 %. For these structures, higher dose values are found when the heterogeneous model is considered. For the other eye structures, the higher doses are determined when the homogeneous water eye model is taken into consideration.

Applicators models CCA and CCB are the most used for treatments of choroidal melanomas of small size; however, published experimental data for these applicators are scarce, owing to the difficulties entailed in measuring small irradiated fields. The simulated ^{106}Ru/Rh^{106} applicators seem to be effective for the treatment concerned. Because of the ^{106}Ru/Rh^{106} applicators dosimetric characteristics, some care must be taken to ensure adequate coverage of the tumor volume. Choroidal and uveal melanomas are relatively resistant to irradiation; thus, the brachytherapy doses needed to control these tumors are associated with a substantial risk of radiation damage in the critical structures. Larger tumors (>5mm) and more anterior ones are more likely to develop complication after brachytherapy treatment, once these parameters affect the radiation dose to the lens, optic disc and macula/fovea.

In present work, considering the chosen tumor i.e. its localization region, thickness and volume, the CCA applicator presented better results, namely the dose delivered to critical structures were lower. However, the important point is to know the behavior of isodoses generated by both applicators in order to decide the appropriate one to be used according to the tumor to treated, its localization and dimensions. Without knowing the scenario to be considered, it isn't possible to elect the best plaque to be applied.

The use of the treatment planning system together with Monte Carlo simulations would be the best procedure for ophthalmic brachytherapy planning. However, this is a procedure difficult to be followed in common radiotherapy centers. In many ophthalmic brachytherapy centers, mainly localized in underdeveloped and developing countries, no treatment planning for ophtalmologic brachytherapy is carried out. Treatment doses are determined using doses values obtained from the source calibration certificate, corrected for the source radioactive decay. Therefore, the eye model developed in this work and the doses distribution determined in the present investigation are of high importance to give to the physician an idea of dose distributions involved in the treatment. Additionally, the method permits calculations for additional tumor localizations, aiming the calculation of doses.

Conflict of interest

The authors declare that they have no conflicts of interest. The authors alone are responsible for the content and writing of the paper.

Acknowledgements

References

1. ICRU 72. Dosimetry of beta rays and low-energy photons for brachytherapy with sealed sources. *J ICRU* 2004; **4**:5-8.
2. Schueler AO, Flühs D, Anastassiou G, *et al.* Beta-ray brachytherapy with 106Ru plaques for retinoblastoma. *Int J Radiat Oncol Biol Phys* 2006; **65**: 1212-21.
3. Lommatzsch PK, Werschnik C, Schuster E. Long-term follow-up of Ru-106/Rh-106 brachytherapy for posterior uveal melanoma. *Graefes Arch Clin Exp Ophthalmol* 2000; **238**: 129-37.
4. Lommatzsch PK. ß-irradiation of choroidal melanoma with 106Ru/106Rh- Applicators.16 years' experience. *Arch Ophthalmol* 1983; **101**: 713-7.
5. Tjho-Heslinga RE, Kakebeeke-Kemme HM, Davelaar J, *et al.* Results of ruthenium irradiation of Uveal melanoma. *Radiotherapy Oncol* 1993; **29**: 33–8.
6. Verschueren KM, Creutzberg CL, Schalij-Delfos NE, *et al.* Long-term outcomes of eye-conserving treatment with Ruthenium (106) brachytherapy for choroidal melanoma. *Radiother Oncol* 2010; **95**: 332–8.
7. Seregard S. Long-term survival after ruthenium plaque radiotherapy for uveal melanoma. A metaanalysis of studies including 1,066 patients. *Acta Ophthalmol Scand* 1999; **77**: 414-7.
8. Damato B, Patel I, Campbell IR, *et al.* Visual acuity after Ruthenium (106) brachytherapy of choroidal melanomas. *Int J Radiat Oncol Biol Phys* 2005; **63**: 392-400.
9. Kirwan JF, Constable PH, Murdoch IE, Khaw PT. Beta irradiation: new uses for an old treatment: a review. *Eye* 2003; **17**: 207-15.
10. Nag S, Quivey JM, Earle JD, *et al.* The American Brachytherapy Society Recommendations for brachytherapy of uveal melanomas. *Int J Radiat Oncol Biol Phys* 2003; **56**: 544–55.
11. Singh AD, Topham A. Incidence of uveal melanoma in the United States: 1973-1997. *Ophthalmology* 2003; **110**: 956-61.
12. Wilson MW, Hungerford JL. Comparison of episcleral plaque and proton beam Radiation therapy for the treatment of choroidal melanoma. *Ophthalmology* 1999; **106**: 1579-87.
13. Koch N, Newhauser WD, Titt U, *et al.* Monte Carlo calculations and measurements of Absorbed dose per monitor unit for the treatment of uveal melanoma with proton therapy. *Phys Med Biol* 2008; **53**: 1581–94.
14. Moore RF. Choroidal sarcoma treated by intraocular insertion of radon seeds. *Br J Ophthalmol* 1930; **14**: 145–52.
15. Eckert & Ziegler BEBIG GmbH, User manual Ru-106 eye applicators TD04_002 / Rev. 11/09 2013.
16. COMS. Collaborative Ocular Melanoma Study Group. Manual of Procedures. Accessed from www.jhu.edu/wctb/coms/
17. Freire JE, De Potter P, Brady LW, Longton WA. Brachytherapy in primary ocular tumors. *Semin Surg Oncol* 1997; **13**: 167-76.
18. Finger PT, Lu D, Buffa A, *et al.* Palladium-103 versus Iodine-125 for ophthalmologic plaque radiotherapy. *Int J Rad Oncol Biol Phys* 1993; **27**: 849-54.
19. Thomson RM, Rogers DW. Monte Carlo dosimetry for 125I and 103Pd eye plaque brachytherapy with various seed models. *Med Phys* 2010; **37**: 368-76.
20. Chiu-Tsao ST, Astrahan MA, Finger PT, *et al.* Dosimetry of 125I and 103Pd COMS eye plaques for intraocular tumors: Report of Task Group 129 by the AAPM and ABS. *Med Phys* 2012; **39**: 6161-84.
21. Barbosa NA, da Rosa LAR, Facure A, Braz D. Brachytherapy treatment simulation of stronti-um-90 and ruthenium-106 plaques on small size

posterior uveal melanoma using MCNPX code. *Radiation Physics and Chemistry* 2014; **95**: 224–6.

22. Astrahan MA. A patch source model for treatment planning of ruthenium ophthalmic applicators. *Medical Physics* 2003; **30**: 1219 –28.

23. Soares CG, Vynckier S, Järvinen H, *et al.* Dosimetry of beta-ray ophthalmic applicators: Comparison of different measurement methods. *Med Phys* 2001; **28**: 1373–84.

24. Rivard MJ, Melhus CS, Sioshansi S, Morr J. The impact of prescription depth, dose rate, plaque size, and source loading on the central-axis using 103Pd, 125I, and 131 Cs. *Brachytherapy* 2008; **7**: 327–35.

25. Gleckler M, Valentine JD, Silberstein EB. Calculating lens dose and surface dose rates from 90Sr ophthalmic applicators using Monte Carlo modeling. *Med Phys* 1998; **25**:29–36.

26. Zhang H, Martin D, Chiu-Tsao ST, *et al.* A comprehensive dosimetric comparison between (131)Cs and (125)I brachytherapy sources for COMS eye plaque implant. *Brachytherapy* 2010; **9**: 362 –72.

27. Cross WG, Hokkanen J, Järvinen H, *et al.* Calculation of beta-ray dose distributions from ophthalmic applicators and comparison with measurements in a model eye. *Med Phys* 2001; **28**: 1385–96.

28. Chiu-Tsao S, O'Brien K, Sanna R, *et al.* Monte Carlo dosimetry for 125I and 60Co in eye plaque therapy. *Med Phys* 1986; **13**: 678–82.

29. Fuss MC, Muñoz A, Oller JC, *et al.* Energy de¬position by a 106Ru/106Rh eye applicator simulat¬ed using LEPTS, a low-energy particle track simula¬tion. *Appl Radiat Isot* 2011; **69**:1198–204.

30. Pelowitz DB. MCNPXTM User's Manual Version 2.5.0. Los Alamos National Laboratory report LA-CP-05-0369. 2005.

31. Briesmeister J F. A General Monte Carlo code for neutron and photon transport, Version 3A. Los Alamos, NM, Los Alamos National Laboratory, LA-12625-M.March. 1997.

32. Davelaar J, Schaling DF, Hennen LA, Broerse JJ. Dosimetry of ruthenium-106 eye applicators. *Med Phys* 1992; **19**: 691–4.

33. Brualla L, Sempau J, Sauerwein W. Comment on Monte Carlo calculation of the dose distributions of two 106Ru eye applicators [Radiother Oncol 1998: 49; 191-196]. *Radiother Oncol* 2012; **104**: 267–8.

34. Chan MF, Fung AY, Hu YC, *et al.* The measurement of three dimensional dose distribution of a ruthenium-106 ophthalmological applicator using magnetic resonance imaging of BANG polymer gels. *J Appl Clin Med Phys* 2001; **2**: 85–9.

35. ICRP PUBLICATION 89. Basic Anatomical and Physiological Data for Use in Radiological Protection: Reference Values. Editor J. VALENTIN. International Commission on Radiological Protection. 2003.

36. ICRU 46. Photon, Electron, Photon and Neutron Interaction Data for Body Tissues. DC Washington 1992.

37. Hermida-López M. Calculation of dose distributions for 12 106Ru/106Rh ophthalmic applicator models with the PENELOPE Monte Carlo code. *Med Phys* 2013; **40**: 101705.

38. Marconi DG, Castro DG, Rebouças LM, et al. Tumor control, eye preservation and visual outcomes of ruthenium plaque brachytherapy for choroidal melanoma. *Brachytherapy* 2013; **12**: 235-9.